Ocean Dynamics (2009) 59:477–488
DOI 10.1007/s10236-009-0182-9

Multi-core structure of the Kuroshio in the East China Sea from long-term transect observations

Hong-Xia Chen · Fang-Li Qiao · Tal Ezer · Ye-Li Yuan · Feng Hua

Received: 4 February 2009 / Accepted: 10 February 2009 / Published online: 10 March 2009

Abstract Long-term hydrographic temperature and salinity transect data in the East China Sea from June 1955 to November 2001 are analyzed in order to examine the geostrophic velocity and the structure of the Kuroshio current. The structure of the Kuroshio Current is divided into three basic forms, a single-core structure, a double-core structure and a multi-core structure; the appearance percentage of the three forms are 53.1%, 31.4%, and 15.4%, respectively. The analysis suggests that multi-core structures have significant seasonal and interannual variabilities that are not fully understood but may relate to variations in transport and associated flow instabilities. The Kuroshio's spatial character is also analyzed in detail by applying a simplified model of motion instability into this multi-core structure of the East China Sea Kuroshio. The theoretical results are found to be consistent with the observations, suggesting that the instability of the Kuroshio in the East China Sea may bring forth the formation of the observed multi-core structure.

Keywords East China Sea · Kuroshio · G–PN line · Motion instability · Multi-core structure

Responsible Editor: Anthony C. Hirst

H.-X. Chen (✉) · F.-L. Qiao · Y.-L. Yuan · F. Hua
Key Laboratory of Marine Science and Numerical Modeling,
The First Institute of Oceanography,
State Oceanic Administration,
Qingdao, China
e-mail: chenhx@fio.org.cn

F.-L. Qiao
e-mail: qiaofl@fio.org.cn

Y.-L. Yuan
e-mail: yuanyl@fio.org.cn

F. Hua
e-mail: huaf@fio.org.cn

T. Ezer
Center for Coastal Physical Oceanography,
Old Dominion University,
Norfolk, VA, USA
e-mail: tezer@odu.edu

1 Introduction

1.1 The observed Kuroshio in the East China Sea

Off the east coast of the Taiwan Island, the Kuroshio strides over the Ilan Ridge and flows into the East China Sea, where it encounters the continental break. The Kuroshio then turns right and flows along the Okinawa Trough; its main axis does not show significant swaying there due to topographic restrictions. This stream continuously flows eastward southwest of Kyushu and feeds into the sea south of Japan. This section of the Kuroshio is named as "the East China Sea Kuroshio". The East China Sea Kuroshio is influenced by two important topographic features. One is located at the northeast of Taiwan where the Kuroshio intrudes the continent slope, and the other one is located at the bifurcation point of the Tsushima warm current. Between these two locations, the Kuroshio flow is observed to be quite steady.

Section G–PN locates at the northwest of Okino Erabu Island. It transversely cuts across the trunk of the Kuroshio in the central East China Sea and spans through the Okinawa Trough, the continental slope, and the continental shelf; the inclination angle between the transect and the latitudinal line is about 37° (see the position of section G and section PN in Fig. 1).

Since 1955, regular surveys along this section, which was named as "G line" at that time, have been carried out

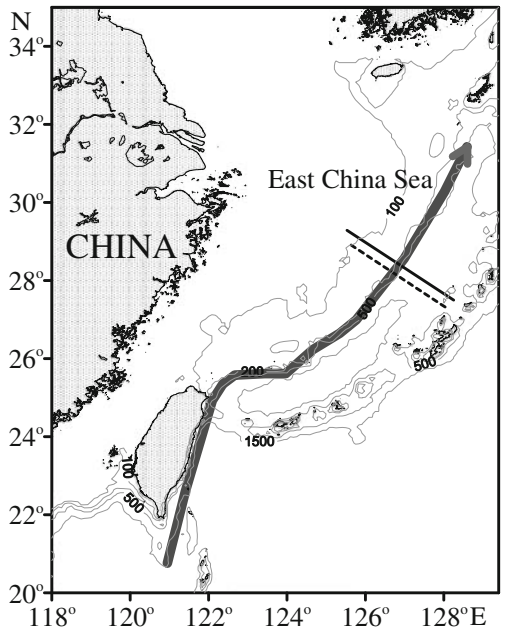

Fig. 1 Spatial position of section G and section PN. The *solid line* represents section PN and the *dash line* represents section G. *Contours* represent isobaths and the *gray thick line* with an *arrow* represents the track of the Kuroshio

by the Oceanic Observatory of Nagasaki, Japan. Annual surveys were conducted in both summer and winter until June 1972, while spring and autumn observations were rarely made in this period. In May 1972, this survey section was renamed as "PN line". This section is parallel to the original "G line", with a small shift to the northeast. Seasonal surveys have been conducted annually since then.

The most stable portion of the Kuroshio is located near the PN section (Sun and Kaneko 1993). The flow direction, the location of the main stream axis, and the width of the Kuroshio are also found stable at the G section, where the maximum survey velocity varies from 0.45 to 1.5 m s^{-1} with an average value of 0.95 m s^{-1} during 1956–1975 (Guan et al. 1979). The flux variation of the Kuroshio shows a seasonal pattern. The volume transport is highest in summer and lowest in autumn, with an average flux of about 28.6 Sv (1 Sv=$10^6 m^3$ s^{-1}) in ten voyages at PN line (Yuan et al. 1991). During 1967–1995, the volume transport of the Kuroshio reached maximums during El Nino event (Kawabe 2001). Although the stream axis of the Kuroshio is relatively stable at the G–PN section, seasonal variations of the axis were indeed observed (Sun 1987). The analysis shows that the energy of eddies, which are generated by baroclinic instability, is supplied by the mean flow (Holland and Lin 1975).

Multi-core structure in the velocity field is one of the intriguing characteristics seen in transects of the East China Sea Kuroshio. Its property and temporal variations are hot research topics now. Akamatsu (1979) was the first to report the multi-core structure of the Kuroshio. He pointed out that there exist three or four cores in the Kuroshio Current profiles at PN line in January, April, July, and September of 1978 (they occurred in February 12–14, April 30–May 2, July 14–15, and October 16–18). This finding reveals clearly that there are three to four subdivided high-flow streams instead of only one. Numerous studies by Chinese researchers confirmed the existence of a multi-core current structure (Yuan et al. 1991). Based on analysis of the hydrographic data collected on *Chufumaru* between September and October 1987, Yuan found two current cores emerging in the Kuroshio at PN line. Yuan et al. (1996, 1998) further pointed out that the Kuroshio has a single current core at PN line in winter. Two current cores were observed occasionally in other seasons. Sun and Kaneko (1993) mentioned that, from 1986 to 1991, the current profile of the East China Sea Kuroshio shows a pattern of either one core and one sheaf or two cores and two sheaves. Based on seasonal data collected during 1992 and 1994 at PN line, the derived velocity from improved inverse method revealed two current cores in each autumn, one core or/and two cores in other seasons (Liu 1998, 1999).

The above studies indicate clearly that the velocity direction, the axis position, and the Kuroshio's width are relatively stable at G–PN section, although a small variation of the axis is found. Three or four cores in the Kuroshio velocity profile at PN line are indicated once only by Akamatsu (1979). In contrast, the pattern of two current cores appears more often. The maximum velocity of the Kuroshio found at G–PN section is about 1.5 m s^{-1}. Although it is possible to validate and analyze the Kuroshio structure with complete seasonal data at G–PN section, it is still not practical to investigate the Kuroshio meander period directly from these data.

1.2 Theoretical background

Classical linear mechanism of baroclinic instability was considered by Charney (1947) and Eady (1949) to explain the fact that growing disturbances both in the atmosphere and in oceans have preferred scales. The effect of a uniform sloping bottom in the Eady model was included by Blumsack and Gierasch (1972). The most important result was that the flow becomes stable if the bottom slope exceeds the isopycnal slope. Studies of the Gulf Stream near 74° W show that the vertical variations of the potential vorticity gradient and the bottom slope are important, and unstable waves are developed at the depth where the potential vorticity gradient changes from negative to positive (Johns 1988). Xue and Mellor (1993), modifying the Moore and Peltier model (1987) to include topography, studied the effect of downstream topographic changes on

the stability of the Gulf Stream in the South Atlantic Bight and pointed out that the important influence of the continental slope on the Gulf Stream is to reduce baroclinic instability associated with the front. James et al. (1999) applied the Xue and Mellor's model to the East China Sea Kuroshio. Model results showed that the instability of the Kuroshio is different from that of the Gulf Stream and the principal factors are the Kuroshio's greater shelf depth, the core location more over the shelf, and the lesser transport. Following Xue and Mellor (1993) in ignoring the viscosity effect and in starting from the governing equations in sigma coordinates, Yuan et al. (2003) presented a motion instability mechanism for the multi-core structure in the main flow of the East China Sea Kuroshio derived under the additional assumption that the disturbances are without along-stream variation. This mechanism gave an analytical relationship between the formation pattern, growth rate, and core scale to the trough topography, background density, and velocity distribution.

In this paper, we use the motion instability mechanism to study the characteristic meander period based on the data provided by the Japan Oceanic Data Center (JODC). Our analysis is focused on different velocity structures and the multi-core structure property of the Kuroshio at G–PN line. The backwash which occurred on the continent shelf, the counter current of the Kuroshio, and other horizontal characters are beyond the scope of the present study. On the basis of the motion instability mechanism suggested by Yuan et al. (2003) and based on inductive analysis of observation and calculation results, we will adjust the motion instability mechanism and investigate the generation of the multi-core structure in the East China Sea Kuroshio. The data and methods used are described in "Section 2". The velocity distributions of the Kuroshio are examined in "Section 3". In "Section 4", a simplified model for motion instability analysis is introduced and compared with the field observations in the East China Sea. Conclusions are presented in "Section 5".

2 Data and error estimation

All hydrographic data used in this paper, a total of 175 data sets with temperature, salinity, and depth from different voyages from June 1955 to November 2001, are obtained from the JODC website. The data along the G–PN section are between 125° and 130° E covering Okinawa Trough, the continental slope, and part of the continental shelf. The number and distribution of survey stations obviously have temporal variations that need to be considered. All survey stations are evenly distributed from June 1955 to May 1977, and the number of stations is about six to ten. After July 1977, more stations have been added on the continental shelf and slope side of the Kuroshio. The number of stations is increased to nine to 16, as shown in Fig. 2.

Traditionally, a mid-point geostrophic velocity is calculated using raw data at two adjacent stations. In this study, we employed a method of linear distance interpolation from each station to the survey section at longitude of about 125.5° E (in kilometers, all linear distances mentioned hereafter are calculated in such a way) before the current is calculated. Then, a set of raw data from the same survey are interpolated to denser gridded points (horizontally ~10 km and vertically ~1 m) using Kriging method. During the process of interpolation, the following conditions are employed: (1) The extreme values of the interpolated data must be maintained at the survey locations; (2) The extreme of the first-order derivative of the interpolated data must be maintained in the mid location between survey stations; and (3) Those gridded points falling outside the survey are not used.

On the basis of the P-vector method (Chu 1995), Chen et al. (2003) developed a non-linear conjugate gradient method and applied it to geostrophic velocity calculations of the East China Sea Kuroshio with hydrographic data. Their results show that zero velocity exists at depth of about 706 m on the PN section. Therefore, the level of no motion is chosen as the water depth if the water depth is less than 700 m and as 700 m otherwise.

The error of the geostrophic current calculation with a double-core structure case is estimated as follows. When we calculate the geotropic velocity, the maximum calculation error introduced is that between the two adjacent stations with the largest change in bottom depth. Without

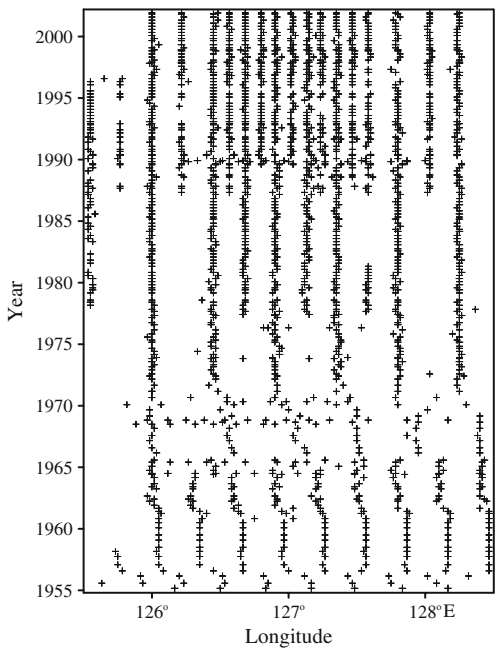

Fig. 2 Stations of long-term transect observations (1955–2001)

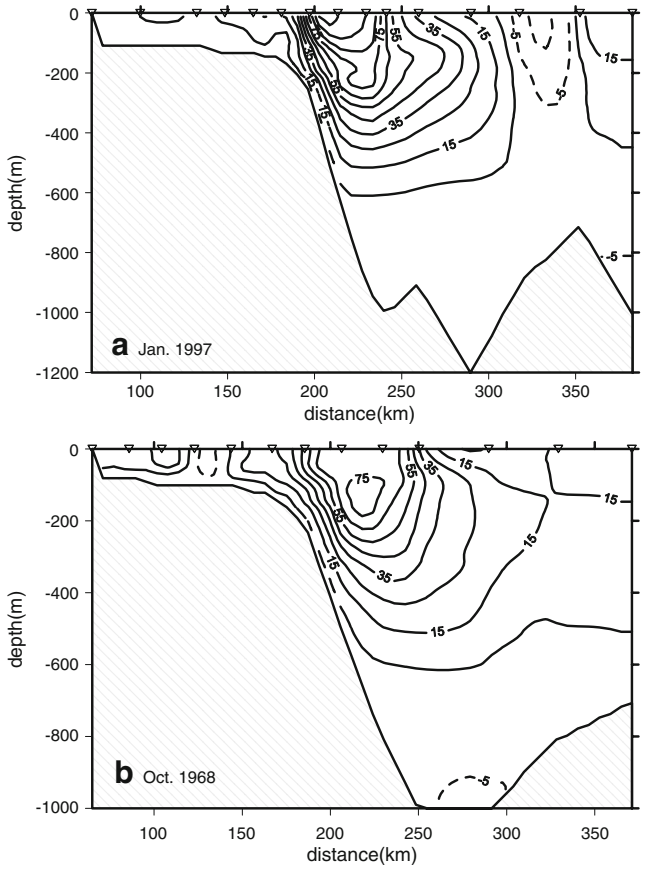

Fig. 3 Examples of single-core velocity structures (time of observations are indicated). *Solid lines* represent positive values (northeastward flow) and *dash lines* represent negative values (southwestward flow). Contour interval is 10 cm s^{-1}

data interpolations, the maximum value of $\partial\rho/\partial x$ is about $0.3\text{kgm}^{-3}/30\text{km} \approx 0.1 \times 10^{-5}\text{kgm}^{-4}$. Considering that the rounded distance in depth is about 550 m, we estimate that the maximum calculation error of the geostrophic velocity is about 0.08 m s^{-1}. Using Kriging interpolation method with several strict qualifications, the maximum calculation error of the geostrophic velocity is now reduced to less than 0.03 m s^{-1} in the extreme conditions. As the value of contour interval of velocity is 0.1 m s^{-1}, we can see that no artificial multi-core structure would be introduced due to the data interpolation. When doing statistic analysis of current cores, the following issues are considered. First, only those cores that occurred in the Kuroshio are taken into account and, second, we make sure that the positions of the current cores are at the geometrical centers of the cores.

3 Velocity distribution in the East China Sea Kuroshio

From the calculated current profiles and current core statistic analysis, we can see that the current structure of the East China Sea Kuroshio have several basic forms as listed below:

Single-core structure: There are 93 sets with a single current core among all 175 data sets which account for 53.1%. The most obvious character of a single-core structure is that there exists only one current core with high velocity and positive direction in the Kuroshio, as shown in Fig. 3. We can see that the current core

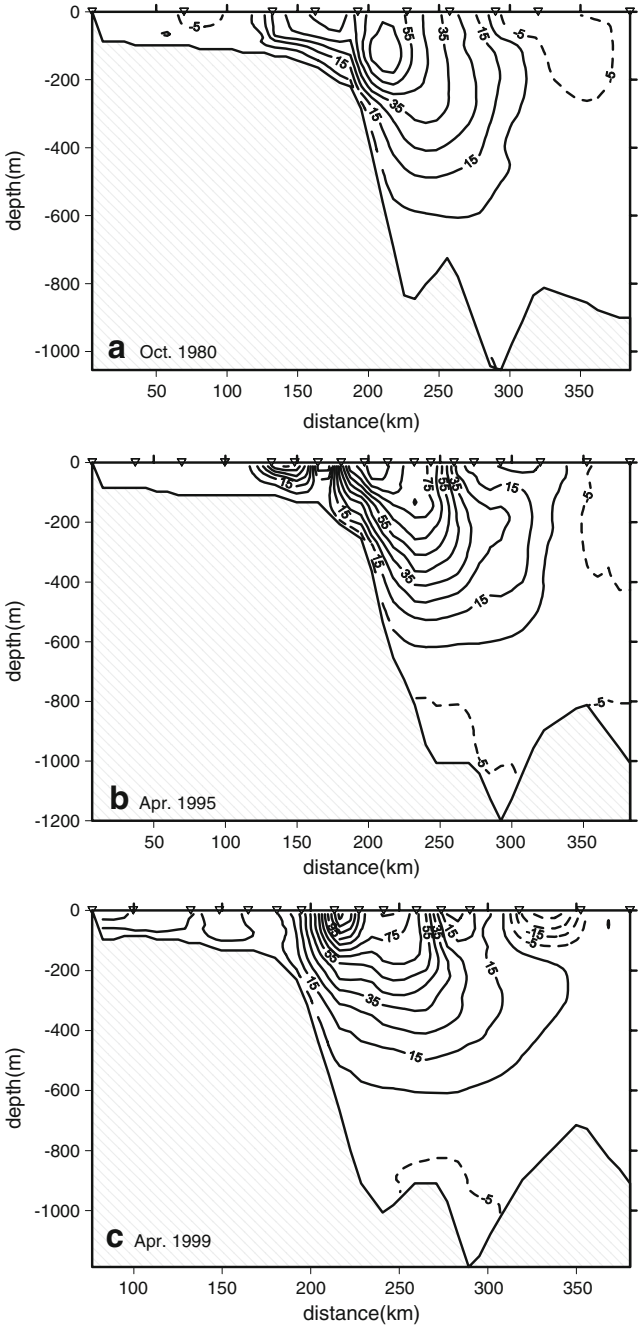

Fig. 4 Same as Fig. 3 but for double-core velocity structures

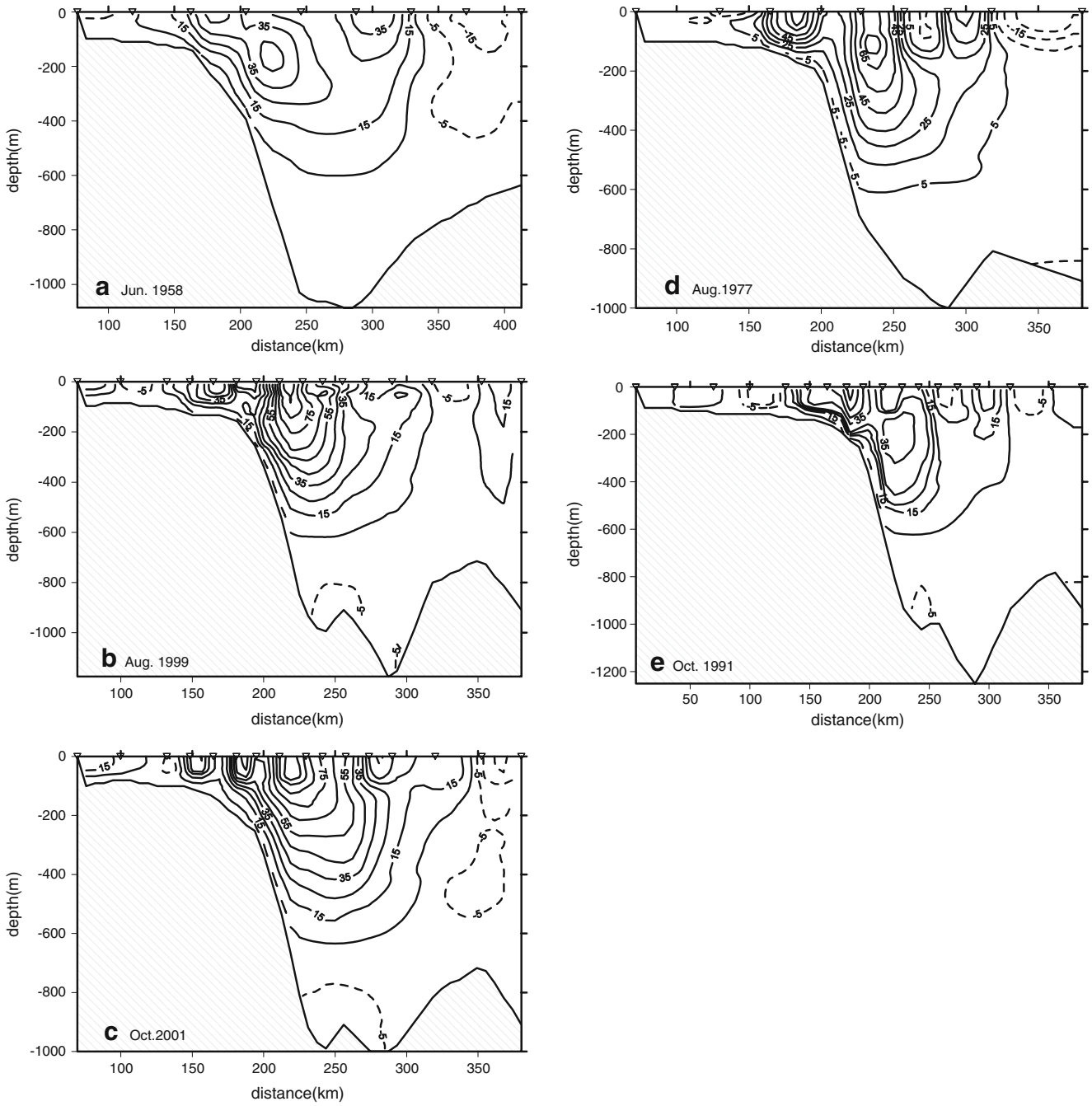

Fig. 5 Same as Fig. 3 but for multi-core velocity structures

situates at the continental slope. Velocity gradients are larger on the left (shoreward) side of the core and smaller on the right (deep ocean) side. Positions of current cores of the single-core structure are pointed out in Fig. 6a, and the positions are comparatively concentrated. Almost all points are located near the position of 220 km and the variance of the position is ±30 km. There are, however, some exceptions. Before 1977, the current cores were often located at less than 190 km distance, which may be a result of coarser resolution in the survey stations.

Double-core structure: About 55 sections in the Kuroshio are found to have two cores which account for 31.4%. The most visible character of the double-core structure is its dual current cores with positive velocities. If we define the core with a higher velocity as the main core, then the main core of double-core structure still lies on the continental slope. According

to the relative positions of these two cores, the double-core structure can be classified into three forms, as shown in Fig. 4. The first form is similar to the single-core structure but with an additional weaker core on the continental shelf side. Both cores of the first form are enveloped by the same contour. The main core of the second form is located on the right side of the core with relatively lower velocity and the two cores are separated by a larger distance (Fig. 4). In the third form, the minor core is found farther away from the continent shelf, while the main core is found on the left, closer to the shelf (Fig. 4). Positions of these double-core structures are shown in Fig. 6b, with all current cores located at about 160- to 280-km distance. Compared to the single-core structures, the double-core structures distribute more divergently and the maximum velocity is found at deeper layers (100–200 m) compared with the single-core cases of Fig. 6a.

Multi-core structure: If three or more cores appear in this section, they are called multi-core structure; these cases appeared 27 times and account for 15.4% of the total cases. With the increase of current core number, the current distributions also become more complex and show larger variations. Based on the position and number of current cores, the multi-core structure can also be divided into several forms as shown in Fig. 5. The three-core structure is characterized by two minor cores that are found on both sides of the main core (Fig. 5). Two minor cores rarely emerge at the same side of the main core, either near or far from the continent shelf. The cases with four or five cores are characterized by a main core that is found above the continental slope as in the previous cases but additional minor cores, which are often found at depths less than 100 m (Fig. 5), are scattered in the region 150–300 km (Fig. 6c). Figure 6d shows the distribution of all cores events. Big circles indicate the center of relatively concentrated areas of all current cores, and current cores' concentrated areas lie in the continental shelf region, the continental slope region, and deep-water region respectively from west to east. Besides the continental slope region where the main body of the Kuroshio passes through, more current cores emerge in the continental shelf region than in the deep-water region. This means that the current core has the character of a regional orientation. Generally, the horizontal distance between cores is on average about 38 km. While considering the lopsided condition, the distance between cores is smaller at the near-shelf side (~30 km) than that at the deepwater side (~50 km). From this figure, we can also see that more than 85% of the current cores emerge in the upper 100 m of the water column and most of the other cores emerge in 100- to 200-m depths. This shows that the maximum current of the Kuroshio is usually located below the surface.

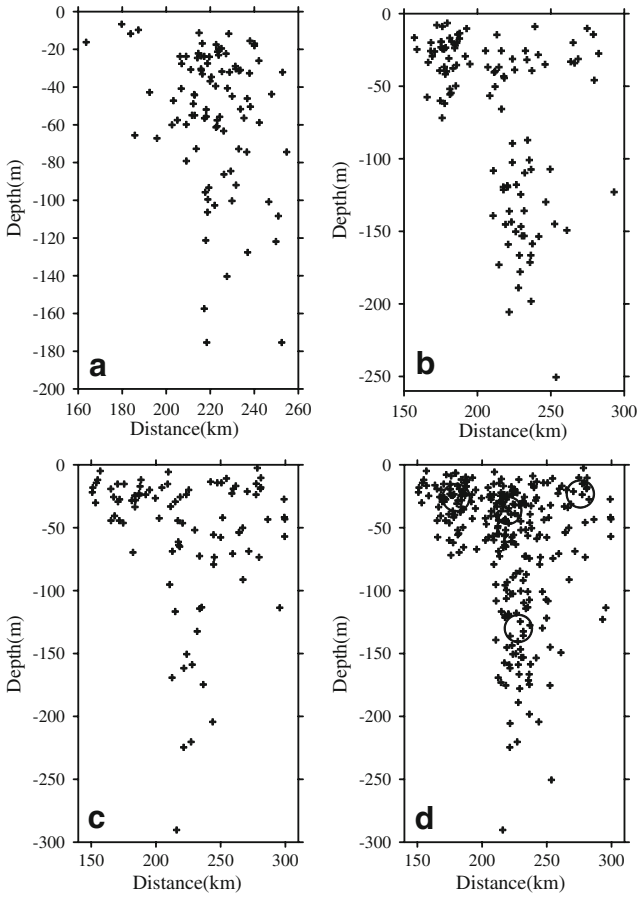

Fig. 6 The distributions of current core positions. Here, each *black cross* signs for a current core while *big black circle* stands for middle points of current core relatively concentrated areas. **a**–**c** Current core distribution of single-core structure, double-core structure, and multi-core structure, respectively. All kinds of current cores are spotted in **d**

Based on the derived velocity of the Kuroshio, the above three forms of single-core, double-core, and multi-core structures all are present in the Kuroshio at the G–PN line; the single-core structure occurs most often, while the multi-core structure the least often, as shown in Fig. 7.

Although all three basic current structures present themselves at the G–PN section, from Fig. 7 we can see that they have obviously seasonal preferences. A single-core structure is found in 75% of the winter observations and in 50% of the spring and summer observations but is the least common structure during the fall season. As for double-core structure, its presence is least frequent in winter and most frequent in autumn. Most of the multi-core structures are present in fall and summer, but it accounts for less than 9% of the cases during winter and spring. Taking into account the spatial distribution and the number of stations, the entire observation time can be divided into four periods: 1955~1965,

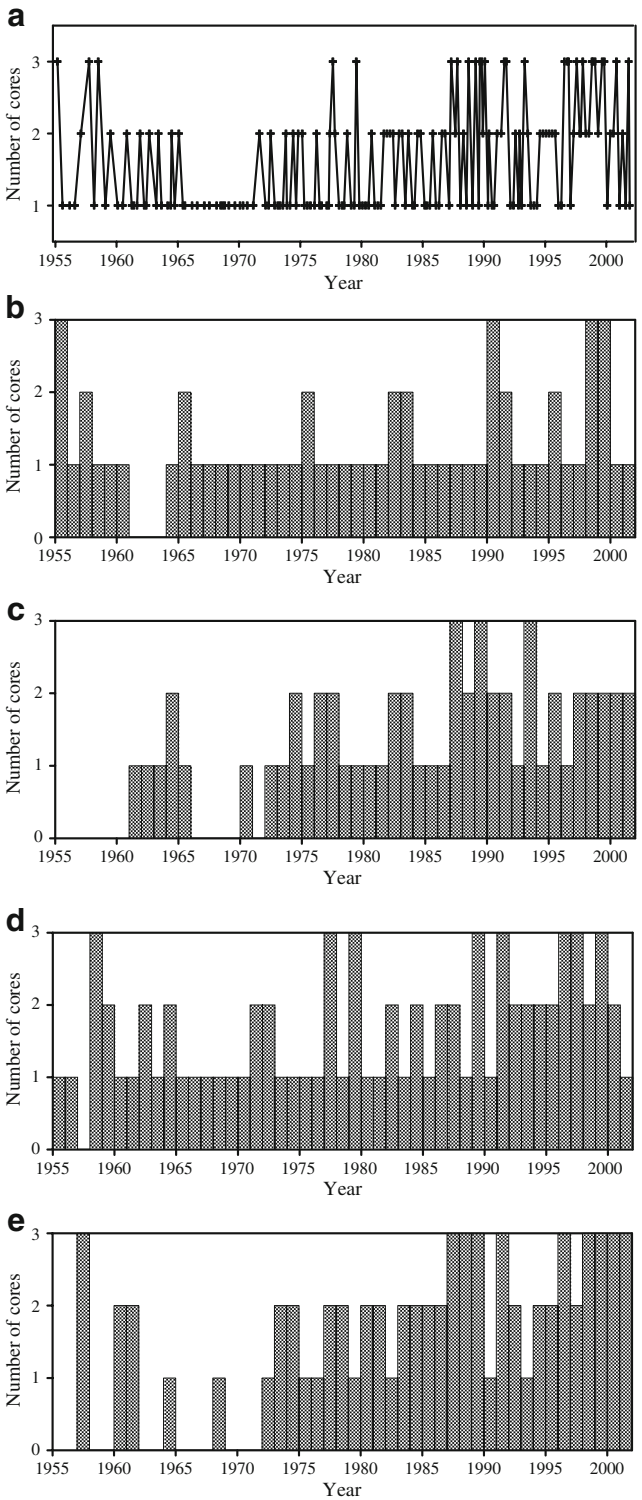

Fig. 7 Core numbers of long-term transect observations (1955–2001). **a** Core number time series of all observations. **b**–**e** Seasonal core number series of winter, spring, summer, and autumn, respectively

1965~1977, 1977~1989, and 1989~2002. In each time period, the velocity structure has respective interannual preferences: (1) During 1955~1965, when the survey stations were evenly distributed and the number of survey stations was about nine, single-core structure accounts for most of the cases, double-core structure appeared now and then, and multi-core structure appeared only three times; (2) During 1965~1977, when the average number of stations was about six, no multi-core structure appeared, so single-core structures maintained for some 7 years (1965~1971); (3) After 1977, when more stations have been added near the continental shelf and slope, multi-core structure reappeared for five times and double-core structure occurred most often during 1982~1984; (4) When the number of survey stations increased from nine to 16, more multi-core structure appeared during 1989~2002 and almost no single-core structure appeared in 1997~1999.

Statistically, all current sections of the Kuroshio on PN section can be decomposed qualitatively into two components: one is an averaged current that can be considered as the background field and the other is current deviation from the background field that represents the multi-core structure. The background field is a steady flow with higher velocity in the top layer and lower velocity in deep layers. The background field is about 500 m in thickness with a typical width of about 150 km. The multi-core current field, which often exists within the top 150 m, is a fluctuation that is superimposed on top of the background field. Note also that current cores are often closer to the shelf side than to the deep ocean side.

4 Simplified model and its application

4.1 Presentation of the problem

The Kuroshio is a strong western boundary current with horizontal fronts on both sides and a large ratio between its width and depth. The perturbations are considered in the meso-scale range, thus, under the Boussinesq, hydrostatic, incompressible, and adiabatic approximations, the governing equations in the σ- coordinate $\left\{x_1 = x_{10}, x_2 = x_{20}, \sigma = \frac{x_{30}-\zeta}{H+\zeta}\right\}$ are written as follows

$$\frac{\partial \zeta}{\partial t} + \frac{\partial (H+\zeta)u_\alpha}{\partial x_\alpha} + \frac{\partial (H+\zeta)\varpi}{\partial \sigma} = 0, \tag{1}$$

$$\frac{\partial u_\beta}{\partial t} + u_\alpha \frac{\partial u_\beta}{\partial x_\alpha} + \varpi \frac{\partial u_\beta}{\partial \sigma} - f\varepsilon_{\beta\gamma 3}u_\gamma = -\frac{1}{\rho_0}\frac{\partial p}{\partial x_\beta} - g\left[\sigma \frac{\partial H}{\partial x_\beta} + (1+\sigma)\frac{\partial \zeta}{\partial x_\beta}\right], \tag{2}$$

$$\frac{\partial p}{\partial \sigma} = -g\rho_0(H+\zeta), \tag{3}$$

$$p(0) = p_0, \tag{4}$$

$$\varpi(0)=0,\varpi(-1)=0, \tag{5}$$

where $\varepsilon_{\alpha\beta\gamma}$ is a 3D unit tensor, all of the symbols used are defined as usual, $x_{30}=\zeta(x_{10},x_{20},t_0)$ and $x_{30}=-H(x_{10},x_{20})$ are the sea surface elevation and the bottom topography, respectively, p_0 is the atmosphere pressure, and assumed $p_0=0$ in the paper. The relationship between the vertical velocity ϖ in σ- coordinate and that u_3 in original one is

$$\varpi=\frac{1}{H+\zeta}\left[u_3-\sigma\left(\frac{\partial H}{\partial x_\alpha}u_\alpha\right)-(1+\sigma)\left(\frac{\partial\zeta}{\partial t}+\frac{\partial\zeta}{\partial x_\alpha}u_\alpha\right)\right]. \tag{6}$$

The motion can be divided into two parts, the average part and the perturbation one. The average part is the Kuroshio flow $\{0, U_2(x_1,\sigma), 0, P(x_1,\sigma), \rho_0(x_1,\sigma), Z(x_1)\}$ assumed 2D in space and 1D in motion, and the perturbation part $\{u_1(x_1,\sigma), u_2(x_1,\sigma), \varpi(x_1,\sigma), p(x_1,\sigma), h(x_1)\}$ is assumed 2D in space and 3D in motion. Then, we have governing equations for them as follows:

1. Governing equations for the average part

$$\frac{\partial Z}{\partial t}=0,\ \frac{\partial U_2}{\partial t}=0, \tag{7}$$

$$-fU_2=-\frac{1}{\rho_0}\frac{\partial P}{\partial x_1}-g\left[\sigma\frac{\partial H}{\partial x_1}+(1+\sigma)\frac{\partial Z}{\partial x_1}\right], \tag{8}$$

$$\frac{\partial P}{\partial\sigma}=-g\rho_0(H+Z). \tag{9}$$

This is the geostrophic-static relation between $\{U_2, P\}$ and $\{Z, H, \rho_0\}$, where U_2 is the velocity of the Kuroshio main flow, P the pressure, Z the surface elevation, H the bottom topography, and ρ_0 the sea water density.

2. Governing equations for the perturbation part

Assuming that the perturbations are independent of the x_2-coordinate, we have linearized the governing equations

$$\frac{\partial h}{\partial t}+\overline{H}\frac{\partial u_1}{\partial x_1}+\frac{\partial\overline{H}}{\partial x_1}u_1+\overline{H}\frac{\partial\varpi}{\partial\sigma}=0, \tag{10}$$

$$\frac{\partial u_1}{\partial t}-fu_2=-\frac{1}{\rho_0}\frac{\partial p}{\partial x_1}-g(1+\sigma)\frac{\partial h}{\partial x_1}, \tag{11}$$

$$\frac{\partial u_2}{\partial t}+\left(\frac{\partial U_2}{\partial x_1}+f\right)u_1+\frac{\partial U_2}{\partial\sigma}\varpi=0, \tag{12}$$

$$\frac{\partial p}{\partial\sigma}=-g\rho_0 h, \tag{13}$$

$$p(0)=0,\varpi(0)=0, \tag{14}$$

$$\varpi(-1)=0, \tag{15}$$

in which $\overline{H}\equiv H+Z$ is the water depth. Due to the set of equations and boundary conditions 10, 11, 12, 13, 14, and 15, the variables $\{u_1, u_2, \varpi, p, h\}$ are over-determined. Therefore, we can derive the solvable conditions first and then find the solutions under the desired conditions.

Before getting the solution we simplify Eqs. 11 and 13. Under condition 14, making $\int_\sigma^0(13)d\sigma$, we have

$$p=g\left(\int_\sigma^0\rho_0\partial\sigma\right)h, \tag{16}$$

and, substituting Eq. 16 into Eq. 11, we get

$$\frac{\partial u_1}{\partial t}-fu_2=-g\left(Ah+B\frac{\partial h}{\partial x_1}\right), \tag{17}$$

in which

$$A\equiv\frac{1}{\rho_0}\int_\sigma^0\frac{\partial\rho_0}{\partial x_1}d\sigma, B\equiv1+\sigma+\frac{1}{\rho_0}\int_\sigma^0\rho_0 d\sigma. \tag{18}$$

Now, our problem is represented by Eqs. 10, 11, 12, 13, 14, 15, 16 and 17.

4.2 Solvable condition, dispersion relation and growth rate

1. Solvable conditions

The unified form of vertical eddies and horizontal sub-circulations can be written as

$$\begin{aligned}&u_1=\int_k\mu_1(\varepsilon x_1,\sigma)\exp\{ik(x_1-ct)\}dk, u_2=\int_k\mu_2(\varepsilon x_1,\sigma)\exp\{ik(x_1-ct)\}dk\\&\varpi=\int_k v(\varepsilon x_1,\sigma)\exp\{ik(x_1-ct)\}dk, h=\int_k\eta(\varepsilon x_1,\sigma)\exp\{ik(x_1-ct)\}dk\ .\end{aligned} \tag{19}$$

Here, amplitudes are assumed to be slowly varied with the x_1 coordinate, as functions of εx_1 with small dimensionless parameter ε. Substituting Eq. 19 into Eqs. 10, 17, 12, 14, and 15, we have

$$-ikc\eta + \left(ik\overline{H} + \frac{\partial \overline{H}}{\partial x_1}\right)\mu_1 + \overline{H}\frac{\partial v}{\partial \sigma} = 0, \tag{20}$$

$$-ikc\mu_1 - f\mu_2 = -g(A + ik_1 B)\eta, \tag{21}$$

$$-ikc\mu_2 + \left(\frac{\partial U_2}{\partial x_1} + f\right)\mu_1 + \frac{\partial U_2}{\partial \sigma}v = 0, \tag{22}$$

$$v(0) = 0, \tag{23}$$

$$v(-1) = 0. \tag{24}$$

Solving Eqs. 20 and 21, we have

$$\mu_1 = \frac{\partial U_2}{\partial \sigma}\frac{f}{\Omega^2}v - ig\overline{A}\frac{kc}{\Omega^2}\eta, \tag{25}$$

$$\mu_2 = -i\frac{\partial U_2}{\partial \sigma}\frac{kc}{\Omega^2}v - g\overline{A}\left(1 + \frac{1}{f}\frac{\partial U_2}{\partial x_1}\right)\frac{f}{\Omega^2}\eta, \tag{26}$$

in which

$$\Omega^2 \equiv \left[(kc)^2 - f\left(f + \frac{\partial U_2}{\partial x_1}\right)\right], \overline{A} \equiv A + ikB, \tag{27}$$

and then, substituting Eq. 25 into Eq. 20, we get the first-order equation of v

$$\frac{\partial v}{\partial \sigma} + ik\left(1 - i\frac{\partial \overline{H}}{k\overline{H}\partial x_1}\right)\frac{f}{\Omega^2}\frac{\partial U_2}{\partial \sigma}v + kc\left[\frac{gk\overline{A}}{\Omega^2}\left(1 - i\frac{\partial \overline{H}}{k\overline{H}\partial x_1}\right) - i\frac{1}{\overline{H}}\right]\eta = 0. \tag{28}$$

The solution of Eq. 28 under condition 24 can be easily written as

$$v = -\exp\left\{-i\int_{-1}^{\sigma}\frac{fk}{\Omega^2}\left(1 - i\frac{1}{k\overline{H}}\frac{\partial \overline{H}}{\partial x_1}\right)\frac{\partial U_2}{\partial \sigma}d\sigma\right\}x \int_{-1}^{\sigma}\left[\frac{gk\overline{A}}{\Omega^2}\left(1 - i\frac{1}{k\overline{H}}\frac{\partial \overline{H}}{\partial x_1}\right) - i\frac{1}{\overline{H}}\right](kc\eta) \exp\left\{i\int_{-1}^{\sigma}\frac{fk}{\Omega^2}\left(1 - i\frac{1}{k\overline{H}}\frac{\partial \overline{H}}{\partial x_1}\right)\frac{\partial U_2}{\partial \sigma}d\sigma\right\}d\sigma \tag{29}$$

Substituting Eq. 29 into Eq. 23 and removing the first factor and factors which are not equal to zero, we have the required solvable condition

$$\int_{-1}^{0}\left[\frac{gk\overline{A}\left(1 - i\frac{1}{k\overline{H}}\frac{\partial \overline{H}}{\partial x_1}\right)}{(kc)^2 - f\left(f + \frac{\partial U_2}{\partial x_1}\right)} - i\frac{1}{\overline{H}}\right] \exp\left\{i\int_{-1}^{\sigma}\left[\frac{fk\frac{\partial U_2}{\partial \sigma_1}\left(1 - i\frac{1}{k\overline{H}}\frac{\partial \overline{H}}{\partial x_1}\right)}{(kc)^2 - f\left(f + \frac{\partial U_2}{\partial x_1}\right)}\right]_{\sigma=\sigma_1} d\sigma_1\right\}d\sigma = 0. \tag{30}$$

Obtaining this solvable condition in the form of an integral equation is a great result but not easy to use. In order to get approximate conditions in algebra form, we introduce a reasonable assumption that the parameters which appeared in Eq. 30 are all slowly varied function of σ and then get the approximate solvable condition

$$\left[\frac{gk\overline{A}\left(1 - i\frac{1}{k\overline{H}}\frac{\partial \overline{H}}{\partial x_1}\right)}{(kc)^2 - f\left(f + \frac{\partial U_2}{\partial x_1}\right)} - i\frac{1}{\overline{H}}\right]_{\sigma=\sigma_0} \times \int_{-1}^{0}\exp\left\{i\left[\frac{fk\frac{\partial U_2}{\partial \sigma_1}\left(1 - i\frac{1}{k\overline{H}}\frac{\partial \overline{H}}{\partial x_1}\right)}{(kc)^2 - f\left(f + \frac{\partial U_2}{\partial x_1}\right)}\right]_{\sigma=\sigma_0}\sigma\right\}d\sigma = 0, \tag{31}$$

where σ_0 is an integral middle value. In the approximate solvable condition, we focus on the approximate solvable condition:

$$\int_{-1}^{0}\exp\left\{i\left[\frac{fk\frac{\partial U_2}{\partial \sigma_1}\left(1 - i\frac{1}{k\overline{H}}\frac{\partial \overline{H}}{\partial x_1}\right)}{(kc)^2 - f\left(f + \frac{\partial U_2}{\partial x_1}\right)}\right]_{\sigma=\sigma_0}\sigma\right\}d\sigma = 0. \tag{32}$$

2. Dispersion relations and growth rates

In the following, we will derive the dispersion relations and growth rates based on the approximate solvable condition 32.

Completing the integral operation of the second approximate solvable condition 32, we get

$$\frac{fk\left(\frac{\partial U_2}{\partial \sigma}\right)_0\left(1 - i\frac{1}{k\overline{H}}\frac{\partial \overline{H}}{\partial x_1}\right)}{(kc)^2 - f\left(f + \frac{\partial U_2}{\partial x_1}\right)_0} = -2\pi N(N > 0, \text{ and it is an integer}). \tag{33}$$

As N=1, it is

$$(kc)^2 = f\left(f + \frac{\partial U_2}{\partial x_1}\right)_0 - \frac{fk}{2\pi}\left(\frac{\partial U_2}{\partial \sigma}\right)_0 + i\frac{f}{2\pi}\left(\frac{\partial U_2}{\partial \sigma}\right)_0\frac{1}{\overline{H}}\frac{\partial \overline{H}}{\partial x_1}. \tag{34}$$

In fact, there are the following scale relationships of perturbations to the surrounding in the Kuroshio area

$$|k| \gg 2\left|\frac{1}{\rho_{00}}\int_{\sigma_0}^{0}\frac{\partial\rho_0}{\partial x_1}d\sigma\right| \text{ and } |k| \gg 2\left|\frac{1}{\overline{H}}\frac{\partial\overline{H}}{\partial x_1}\right|. \tag{35}$$

We have

$$\left|\frac{k}{2\pi}\left(\frac{\partial U_2}{\partial\sigma}\right)_0\right| \gg 2\left|\frac{1}{2\pi}\left(\frac{\partial U_2}{\partial\sigma}\right)_0\frac{1}{\overline{H}}\frac{\partial\overline{H}}{\partial x_1}\right|, \quad or \left|\frac{\frac{1}{2\pi}\left(\frac{\partial U_2}{\partial\sigma}\right)_0\frac{\partial\overline{H}}{\overline{H}\partial x_1}}{\left(f+\frac{\partial U_2}{\partial x_1}\right)_0-\frac{k}{2\pi}\left(\frac{\partial U_2}{\partial\sigma}\right)_0}\right| \ll \frac{1}{2}, \tag{36}$$

and then, from Eq. 34, we get the first-order Taylor expansion

$$(kc) = \pm\left[f\left(f+\frac{\partial U_2}{\partial x_1}\right)_0-\frac{fk}{2\pi}\left(\frac{\partial U_2}{\partial\sigma}\right)_0\right]^{1/2}\left[1+i\frac{\frac{1}{2\pi}\left(\frac{\partial U_2}{\partial\sigma}\right)_0\frac{1}{\overline{H}}\frac{\partial\overline{H}}{\partial x_1}}{\left(f+\frac{\partial U_2}{\partial x_1}\right)_0-\frac{k}{2\pi}\left(\frac{\partial U_2}{\partial\sigma}\right)_0}\right]^{1/2}. \tag{37}$$

In the following, we derive the dispersion relations and growth rates in the case that $\left(f+\frac{\partial U_2}{\partial x_1}\right)-\frac{k}{2\pi}\frac{\partial U_2}{\partial\sigma}<0$ Taking the symbol of Eq. 37 making the real part positive, we have

$$(kc) \approx \mathrm{Sign}\left(\frac{\partial\overline{H}}{\partial x_1}\right)\left[\frac{\frac{f}{4\pi}\left(\frac{\partial U_2}{\partial\sigma}\right)_0\frac{\partial\overline{H}}{\overline{H}\partial x_1}}{\left[\frac{fk}{2\pi}\left(\frac{\partial U_2}{\partial\sigma}\right)_0-f\left(f+\frac{\partial U_2}{\partial x_1}\right)_0\right]^{1/2}}+i\left[\frac{fk}{2\pi}\left(\frac{\partial U_2}{\partial\sigma}\right)_0-f\left(f+\frac{\partial U_2}{\partial x_1}\right)_0\right]^{1/2}\right], \tag{38}$$

and then we get the dispersion relation

$$(kc)_D = \frac{1}{4\pi}\frac{\left(\frac{\partial U_2}{\partial\sigma}\right)_0\frac{f}{\overline{H}}\left|\frac{\partial\overline{H}}{\partial x_1}\right|}{\left[\frac{fk}{2\pi}\left(\frac{\partial U_2}{\partial\sigma}\right)_0-f\left(f+\frac{\partial U_2}{\partial x_1}\right)_0\right]^{1/2}}, \tag{39}$$

and the growth rate

$$(kc)_G = \mathrm{Sign}\left(\frac{\partial\overline{H}}{\partial x_1}\right)\left[\frac{fk}{2\pi}\left(\frac{\partial U_2}{\partial\sigma}\right)_0-f\left(f+\frac{\partial U_2}{\partial x_1}\right)_0\right]^{1/2}. \tag{40}$$

4.3 The formation of multi-core structure at PN section in the East China Sea Kuroshio

With the results of Eqs. 39 and 40, we can now discuss the formation mechanism of multi-core structures and calculate scales and distribution of cores at PN section in the East China Sea Kuroshio.

1. The formation of multi-core structures at PN section in the East China Sea Kuroshio

The formation of the Kuroshio multi-core structure is described by the dispersion relation and growth rate derived from the solvable condition 32. In the case of

$$\left(f+\frac{\partial U_2}{\partial x_1}\right)-\frac{k}{2\pi}\frac{\partial U_2}{\partial\sigma} < 0, \text{ or } k > 2\pi\frac{\left(f+\frac{\partial U_2}{\partial x_1}\right)}{\frac{\partial U_2}{\partial\sigma}} > 0, \text{ or } k = 2\pi\frac{2}{3}\frac{\left(f+\frac{\partial U_2}{\partial x_1}\right)_0}{\left(\frac{\partial U_2}{\partial\sigma}\right)_0}, \tag{41}$$

the dispersion relation and growth rate and their variations can be written as

$$(c)_D = \frac{1}{4\pi k}\frac{\left(\frac{\partial U_2}{\partial\sigma}\right)_0\frac{f}{\overline{H}}\left|\frac{\partial\overline{H}}{\partial x_1}\right|}{\left[\frac{fk}{2\pi}\left(\frac{\partial U_2}{\partial\sigma}\right)_0-f\left(f+\frac{\partial U_2}{\partial x_1}\right)_0\right]^{1/2}}, \tag{42}$$

$$\frac{\partial(c)_D}{\partial|k|} = \frac{1}{8\pi}\left(\frac{\partial U_2}{\partial\sigma}\right)_0\frac{f}{\overline{H}}\left|\frac{\partial\overline{H}}{\partial x_1}\right|\left\{\frac{\left[3\frac{fk}{2\pi}\left(\frac{\partial U_2}{\partial\sigma}\right)_0-2f\left(f+\frac{\partial U_2}{\partial x_1}\right)_0\right]}{k^2\left[\frac{fk}{2\pi}\left(\frac{\partial U_2}{\partial\sigma}\right)_0-f\left(f+\frac{\partial U_2}{\partial x_1}\right)_0\right]^{3/2}}\right\}[-\mathrm{Sign}(k)], \tag{43}$$

and

$$(kc)_G = \mathrm{Sign}\left(\frac{\partial\overline{H}}{\partial x_1}\right)\left[\frac{fk}{2\pi}\left(\frac{\partial U_2}{\partial\sigma}\right)_0-f\left(f+\frac{\partial U_2}{\partial x_1}\right)_0\right]^{1/2}, \tag{44}$$

$$\frac{\partial(kc)_G}{\partial|k|} = \mathrm{Sign}\left(\frac{\partial\overline{H}}{\partial x_1}\right)\frac{\frac{f}{4\pi}\left(\frac{\partial U_2}{\partial\sigma}\right)_0}{\left[\frac{fk}{2\pi}\left(\frac{\partial U_2}{\partial\sigma}\right)_0-f\left(f+\frac{\partial U_2}{\partial x_1}\right)_0\right]^{1/2}}[\mathrm{Sign}(k)]. \tag{45}$$

Equations 42, 43, 44, and 45 provide the basis of the formation of the Kuroshio multi-core structure. First, according to Eq. 44, we know that only on the shelf side of the Okinawa trough $\mathrm{Sign}\left(\frac{\partial\overline{H}}{\partial x_1}\right)=1$; the growth rate is positive, so that the flow is unstable and the horizontal sub-circulations would grow up to form the Kuroshio multi-core structure. On the one hand, due to the fact that Eq. 44 is

proportional to the factor $\left[\frac{fk}{2\pi}\left(\frac{\partial U_2}{\partial\sigma}\right)_0 - f\left(f+\frac{\partial U_2}{\partial x_1}\right)_0\right]^{1/2}$ and Eq. 45 is positive, the growth rate is considerably large and the sub-circulations with smaller scales have larger growth rate. On the other hand, due to the fact that Eqs. 42 and 43 are proportional to $\left(\frac{\partial U_2}{\partial\sigma}\right)_0\frac{f}{\overline{H}}\left|\frac{\partial\overline{H}}{\partial x_1}\right|$ and $-\left(\frac{\partial U_2}{\partial\sigma}\right)_0\frac{f}{\overline{H}}\left|\frac{\partial\overline{H}}{\partial x_1}\right|$, respectively, the moving speed of the sub-circulations is always considerably small and the sub-circulation with smaller scales will have smaller moving speed. This means that the sub-circulation in the Kuroshio main flow in the shelf side would have a larger growth rate and a smaller moving speed, allowing it to be developed alongside the main flow. All of these contribute to the development of sub-circulations, and we believe that this is the mechanism in which the multi-core structure is formed.

2. The scaling of multi-core structure at PN section in the East China Sea Kuroshio

According to Eq. 44, the growth rate in unit wave-number can be written as

$$(c)_{\mathrm{G}} = \mathrm{Sign}\left(\frac{\partial\overline{H}}{\partial x_1}\right)\frac{1}{k}\left[\frac{fk}{2\pi}\left(\frac{\partial U_2}{\partial\sigma}\right)_0 - f\left(f+\frac{\partial U_2}{\partial x_1}\right)_0\right]^{1/2}, \tag{46}$$

and then the sub-circulation with maximum growth rate in unit wave-number can be derived from

$$\left.\frac{\partial(c)_{\mathrm{G}}}{\partial k}\right|_{k=k_{\max}} = \mathrm{Sign}\left(\frac{\partial\overline{H}}{\partial x_1}\right) \times \left.\frac{\left[-\frac{fk}{2\pi}\left(\frac{\partial U_2}{\partial\sigma}\right)_0 + 2f\left(f+\frac{\partial U_2}{\partial x_1}\right)_0\right]}{2k^2\left[\frac{fk}{2\pi}\left(\frac{\partial U_2}{\partial\sigma}\right)_0 - f\left(f+\frac{\partial U_2}{\partial x_1}\right)_0\right]^{1/2}}\right|_{k=k_{\max}} = 0, \tag{47}$$

as

$$\begin{aligned} k_{\max} &= 4\pi\frac{\left(f+\frac{\partial U_2}{\partial x_1}\right)_0}{\left(\frac{\partial U_2}{\partial\sigma}\right)_0}, l_{\max} \\ &= \frac{\left(\frac{\partial U_2}{\partial\sigma}\right)_0}{2\left(f+\frac{\partial U_2}{\partial x_1}\right)_0}, (kc)_{\mathrm{Gmax}} \\ &= \mathrm{Sign}\left(\frac{\partial\overline{H}}{\partial x_1}\right)\left[f\left(f+\frac{\partial U_2}{\partial x_1}\right)_0\right]^{1/2}. \end{aligned} \tag{48}$$

We think that this is the most likely condition for the existence of sub-circulations and associated multi-core structures.

The parameters of the Kuroshio main flow can now be estimated as:

$$\begin{aligned} &f \approx 0.7\times10^{-4}\mathrm{s}^{-1}, \partial x_1 = O\left(75\times10^3\mathrm{m}\right), \partial\sigma \\ &= O(0.3), \partial U_2 = O\left(1.5\mathrm{ms}^{-1}\right). \end{aligned} \tag{49}$$

Velocity gradients can be estimated by

$$\begin{aligned} \frac{\partial U_2}{\partial x_1} &= O\left(\frac{\pm1.5\mathrm{ms}^{-1}}{75\times10^3\mathrm{m}}\right) \\ &= O\left((+2.0\sim-2.0)\times10^{-5}\mathrm{s}^{-1}\right), \frac{\partial U_2}{\partial\sigma} \\ &= O\left(\frac{\pm1.5\mathrm{ms}^{-1}}{0.3}\right) = O\left(5.0\mathrm{ms}^{-1}\right), \end{aligned} \tag{50}$$

and the core interval range can be estimated by

$$l_{\max} = \left(\frac{\partial U_2}{\partial\sigma}\right)_0 \Big/ 2\left(f+\frac{\partial U_2}{\partial x_1}\right)_0 = O\left((30\sim50)\times10^3\mathrm{m}\right). \tag{51}$$

These results are quantitatively consistent with the observations and have the property that the core interval is smaller on the shelf side and larger on the open ocean side. Furthermore, taking the time interval in which the sub-circulation grows up about 10^4 times as the growth time scale t_{Gmax} which satisfies the equation $\exp\{(kc)_{\mathrm{Gmax}}\, t_{\mathrm{Gmax}}\} = 10^4$, we have the estimate

$$\begin{aligned} t_{\mathrm{Gmax}} &= \frac{4}{\left(\log_{10}^e\right)\left[f\left(f+\frac{\partial U_2}{\partial x_1}\right)\right]^{1/2}} \\ &= \frac{4}{0.43\times\left[0.7(0.7\pm0.2)\right]^{1/2}}\times10^4\mathrm{s} \\ &= O\left((15\sim26)\times10^4\mathrm{s}\right) \end{aligned} \tag{52}$$

The estimate of growth time is about 2 days. Certainly, this is a reasonable value.

Under the estimate of the scale of the depth variation in the Kuroshio area, we can calculate the moving speed $(c)_{\mathrm{Dmax}}$ and the distance $L_{1\mathrm{day}}$ as follows

$$\begin{aligned} (c)_{\mathrm{Dmax}} &= \frac{1}{(4\pi)^2}\frac{1}{\overline{H}}\left|\frac{\partial\overline{H}}{\partial x_1}\right|\frac{f^{1/2}\left(\frac{\partial U_2}{\partial\sigma}\right)_0^2}{\left(f+\frac{\partial U_2}{\partial x_1}\right)_0^{3/2}} \\ &= O\left((0.5\sim2.2)\times10^{-2}\mathrm{ms}^{-1}\right), \end{aligned} \tag{53}$$

and

$$\begin{aligned} L_{1\mathrm{day}} &\approx 1\mathrm{day}\times24\times60\times60\frac{\mathrm{s}}{\mathrm{day}} \\ &\quad\times\left((0.5\sim2.2)\times10^{-2}\mathrm{ms}^{-1}\right) \\ &\approx (0.4\sim1.9)\mathrm{km}. \end{aligned} \tag{54}$$

This is a considerably small speed and spatial scale, indicating that the sub-circulations have enough time to be developed within the dynamics of the main flow.

5 Conclusions

Although the existence of the multi-core structures in the East China Sea Kuroshio has been reported in numerous previous works, long-term data analysis and multi-core formation mechanisms are still lacking. This work proposes that the current structure in the Kuroshio can be divided into three basic forms, single-core structure, double-core structure and multi-core structure with different appearance percentage at 53.1%, 31.4%, and 15.4%, respectively, based on long-term transect observations (1955~2002). These basic current structures have noticeable seasonal variations. Single-core structure accounts for 75% of the cases during winter, 25% of the cases during fall, and 50% of the cases during spring and summer. For double-core structure, its percentage of occurrence is smallest in winter and highest in autumn. Most of the multi-core structures are found in fall and summer, and it accounts for less than 9% of the cases in winter and spring. Besides the bias associated with the uneven temporal and spatial distribution of the observed stations, the velocity structure has significant interannual variations.

The current profile of the Kuroshio is proposed to be decomposed into two parts: the background current field and the perturbation field. The background field is a steady flow zone with higher flow velocity appearing in the upper layer. The current layer thickness is about 500 m with the maximum velocity of ~1.5 m s^{-1}. The multi-core current field, which often exists within the upper 150 m, is the most unstable perturbation of the background field. The distance between cores is on average about 38 km; the distance is closer at the near-shelf side than that at the deepwater side of the main flow.

The theoretical analysis indicates that the space between cores is consistent with the observations, while the growth time scale and the moving speed calculated from the simplified model suggest that the sub-circulations have enough time to be developed in the main Kuroshio current.

Acknowledgments This work is supported by projects of the National Natural Science Foundation of China (No.40730842 and No. 40506011) and by National Science and Technology Support Plan of China (No. 2006BAB18B02). The temperature and salinity data are obtained from Japan Oceanographic Data Center (JODC).

References

Akamatsu H (1979) Observation of Kuroshio near continent slope in the East China Sea. Marine Science 11:175–181 in Japanese

Blumsack SL, Gierasch PJ (1972) Mars: the effects of topography on baroclinic instability. J Atmos Sci 29:1081–1089

Charney JG (1947) The dynamics of long waves in a baroclinic westerly current. Journal of Meteorology 4:135–163

Chen HX, Yuan YL, Liu N et al (2003) The application of non-linear conjugate gradients method in geostrophic velocity calculation of East China Sea Kuroshio. Acta Oceanologica Sinica 25:31–38 in Chinese

Chu PC (1995) P-vector method for determining ocean circulation from hydrographic data. Mar Technol Soc J 29(3):3–14

Eady ET (1949) Long waves and cyclonic waves. Tellus 1:33–52

Guan B, Liu J, Fan J (1979) Variations of the surface velocity of the Kuroshio on section G in the East China Sea from 1956–1975. Chin Sci Bull 21:990–994

Holland WR, Lin LB (1975) On the generation of mesoscale eddies and their contribution to the oceanic general circulation. J Phys Oceanogr 5:642–669

James C, Wimbush M, Ichikawa H (1999) Kuroshio meanders in the East China Sea. J Phys Oceanogr 29:259–272

Johns WE (1988) One-dimensional baroclinically unstable waves on the Gulf Stream potential vorticity gradient near Cape Hatteras. Dyn Atmos Ocean 11:323–350

Kawabe M (2001) Interannual variations of sea level at the Nansei Islands and volume transport of the Kuroshio due to wind changes. J Oceanogr 57:189–205

Moore GWK, Peltier WR (1987) Cyclogenesis in frontal zones. J Atmos Sci 44:384–409

Liu Y, Yuan Y (1998) Variability of the Kuroshio in the East China Sea in 1992. Acta Oceanologica Sinica 26:1–11 in Chinese

Liu Y, Yuan Y (1999) Variability of the Kuroshio in the East China Sea in 1993 and 1994. Acta Oceanologica Sinica 18:17–36

Sun X (1987) Analysis of the surface path of the Kuroshio in the East China Sea. Papers of the Kuroshio Investigation and Research (in Chinese), pp. 1–14. Ocean Press, Beijing

Sun X, Kaneko I (1993) Variations of the Kuroshio during the period of 1989-1991. In paper selections of the Kuroshio Investigation (IV) (in Chinese), pp 52–68. Ocean, Beijing

Xue H, Mellor G (1993) Instability of the Gulf Stream Front in the South Atlantic Bight. J Phys Oceanogr 23:2326–2350

Yuan Y, Endoh M, Ishizaki H (1991) The study of the Kuroshio in the East China Sea and the currents east of Ryukyu Islands. In paper selections of the Kuroshio Investigation (III) (in Chinese), pp 220–234. Ocean, Beijing

Yuan YC, Kaneko A, Su JL et al (1998) The Kuroshio east of Taiwan and the currents east of the Ryukyu Islands during early summer of 1996. J Oceanogr 54:217–226

Yuan YC, Liu CT, Pan ZQ et al (1996) Circulation east of Taiwan and in the East China Sea and east of the Ryukyu Islands during early summer 1985. Acta Oceanologica Sinica 15(4):423–435

Yuan YL., Wan ZW, Zhang QH (2003) A motion instability formation mechanism of the multi-core structure of the East China Sea Kuroshio. Science in China, Ser D 46(2):182–192